Project No: 603502

DACCIWA

"Dynamics-aerosol-chemistry-cloud interactions in West Africa"

Deliverable

D5.2 Campaign Data

<u>**Due date of deliverable:**</u>	31/05/2017
<u>**Completion date of deliverable:**</u>	31/05/2017

Start date of DACCIWA project:	1st December 2013	**Project duration:**	60 months

Version:	[V1.0]
File name:	[D5.2_Campaign_Data_DACCIWA_v1.0.pdf]

Work Package Number:	**5**
Task Number:	**2**

<u>**Responsible partner for deliverable:**</u>	**UREAD**
Contributing partners:	**KIT, UPS**

Project coordinator name:	Prof. Dr. Peter Knippertz
Project coordinator organisation name:	Karlsruher Institut für Technologie

Dissemination level		
PU	Public	**x**
PP	Restricted to other programme participants (including the Commission Services)	
RE	Restricted to a group specified by the consortium (including the Commission Services)	
CO	Confidential, only for members of the consortium (including the Commission Services)	

Nature of Deliverable		
R	Report	
P	Prototype	
D	Demonstrator	
O	Other	**x**

Copyright

DOCUMENT INFO

Authors

Author	Beneficiary Short Name	E-Mail
Christine Chiu	UREAD	c.j.chiu@reading.ac.uk
Yann Blanchard	UREAD	y.blanchard@reading.ac.uk
Peter Hill	UREAD	p.g.hill@reading.ac.uk
Norbert (IMK) Kalthoff	KIT	norbert.kalthoff@kit.edu
Bianca Adler	KIT	bianca.adler@kit.edu
Fabienne Lohou	UPS	Fabienne.Lohou@aero.obs-mip.fr>

Changes with respect to the DoW

Issue	Comments

Dissemination and uptake

Target group addressed	Project internal / external
Scientific community	Internal and external

Document Control

Document version #	Date	Changes Made/Comments
0.1	15.05.2017	First version to be approved by the general assembly
1.0	31.05.2017	Final version approved by the general assembly

Table of Contents

1. Introduction

This report provides an overview about the cloud product generated from measurements collected in the DACCIWA field campaign in June–July 2016. Detailed cloud microphysical and optical properties, along with atmospheric condition, surface albedo and aerosols, are crucial parameters for accurate radiation prediction at the surface and the top of the atmosphere. Since many studies have reported significant and consistent model biases in radiation (e.g., *Knippertz et al.*, 2011; *Hannak et al.*, 2017) and thus errors in circulation and precipitation (e.g., *Rodwell and Jung*, 2008; *Li et al.*, 2015), this cloud product provides an excellent opportunity to understand cloud evolutions and the sources of cloud biases in models over the DACCIWA region.

Section 2 briefly describes measurements and cloud retrieval method used in the study. Since the retrieval method requires coincident measurements from cloud radar, lidar and shortwave spectral radiometer, main efforts have been made on data from the ground supersite Savé. Section 3 details the content of the cloud product, and takes two examples to highlight the overall performance of the cloud product against other independent datasets including in-situ measurements from aircraft. Finally, some potential issues and plans are outlined.

2. Measurements used in retrieval and radiation closure

2.1 Remote sensing measurements from the supersite Savé

Shortwave zenith radiance measurements provide a crucial constraint on cloud optical depth. Two sunphotometers, supported by the Atmospheric Radiation Measurement (ARM) program Climate Research Facility, were deployed during the DACCIWA campaign. Unlike most sunphotometers that are designed to monitor aerosol properties and thus operated in normal aerosol mode, the sunphotometer at Savé was operated in a special cloud mode, pointing vertically and measuring zenith radiance continuously at wavelengths of 440, 500, 675, 870, 1020 and 1640 nm with 10 sec temporal resolution. Zenith radiances at 440, 870, and 1640 nm alone can be used to retrieve cloud optical depth and column-mean effective radius [*Chiu et al.*, 2010; 2012], but the synergy with radar and lidar measurements makes it possible to provide detailed profiles of cloud water content and droplet size that are critical for understanding cloud processes.

The 35-GHz cloud radar measures reflectivity and Doppler information with a vertical resolution of 30 m and a temporal resolution of 10 sec [see *DACCIWA deliverable, report D01.1*, 2017]. The cloud radar points vertically most of time, except performing Range-Height-Indicator (RHI) scans for ~5 min every 30 min, and special crosswind RHI scans [*Fielding et al.*, 2013] for measuring 3D cloud populations on 2 and 15 July when aircraft flew over Savé. Since it is planned to investigate 3D cloud fields along with in-situ and satellite observations at a later stage of the project, we will focus on cloud radar measurements from the vertical stare mode in this report.

The ceilometer measures backscatter signals at 1064 nm with a 15 m vertical resolution of and a 60 sec temporal resolution. Since lidar backscatter will be completely attenuated by optically thick clouds, the ceilometer is mainly used for determining cloud base height in our retrieval. While cloud base height can be determined in many ways [*Clothiaux et al.*, 1998], we used a backscatter threshold of 0.00005 m^{-1} sr^{-1} to define cloud base for simplicity. This threshold generally corresponds to cloud base height that agrees well with the product provided by the manufacture. Note that for drizzling clouds, the backscatter signals can be used to retrieve precipitation below clouds, as shown in many studies [*O'Connor et al.*, 2005; *Fielding et al.*, 2015].

Surface radiation measurements at Savé are not used in the retrieval process, but they serve two important purposes. One is to derive surface broadband albedo that has been difficult to acquire from satellite observations due to frequent cloudy sky conditions; the other is to serve as a truth to investigate whether retrieved cloud properties can be used to accurately predict surface radiation. During the campaign, there were two surface radiation stations at Savé. The KIT energy balance station is ~10–15 m away from the sunphotometer, and ~50 m from the cloud radar. The UPS energy station is in a similar distance but a different location, providing additional information on the spatial variability of surface albedo and radiation. For both stations, measurements include shortwave (0.4–4 µm) and longwave (4–50 µm) downwelling and upwelling irradiance at a 1-sec temporal resolution.

Figure 1 shows the composite of surface radiation and albedo from these two sites. Among these variables, the downwelling SW irradiance is the most critical variable in this study, showing large daily variations due to complex and fast evolving cloud fields. In general, the SW downwelling irradiances from the two stations agree well, but there are notable differences in SW upwelling and LW irradiances. Further analysis is needed to understand whether the difference is due to instrumentation, or due to the variability of surface type and temperature above the stations. Additionally, Fig. 1(c) and 1(d) suggest a broadband surface albedo of ~0.19 at Savé. This albedo value will be used in our radiative transfer calculations, as discussed in Section 2.
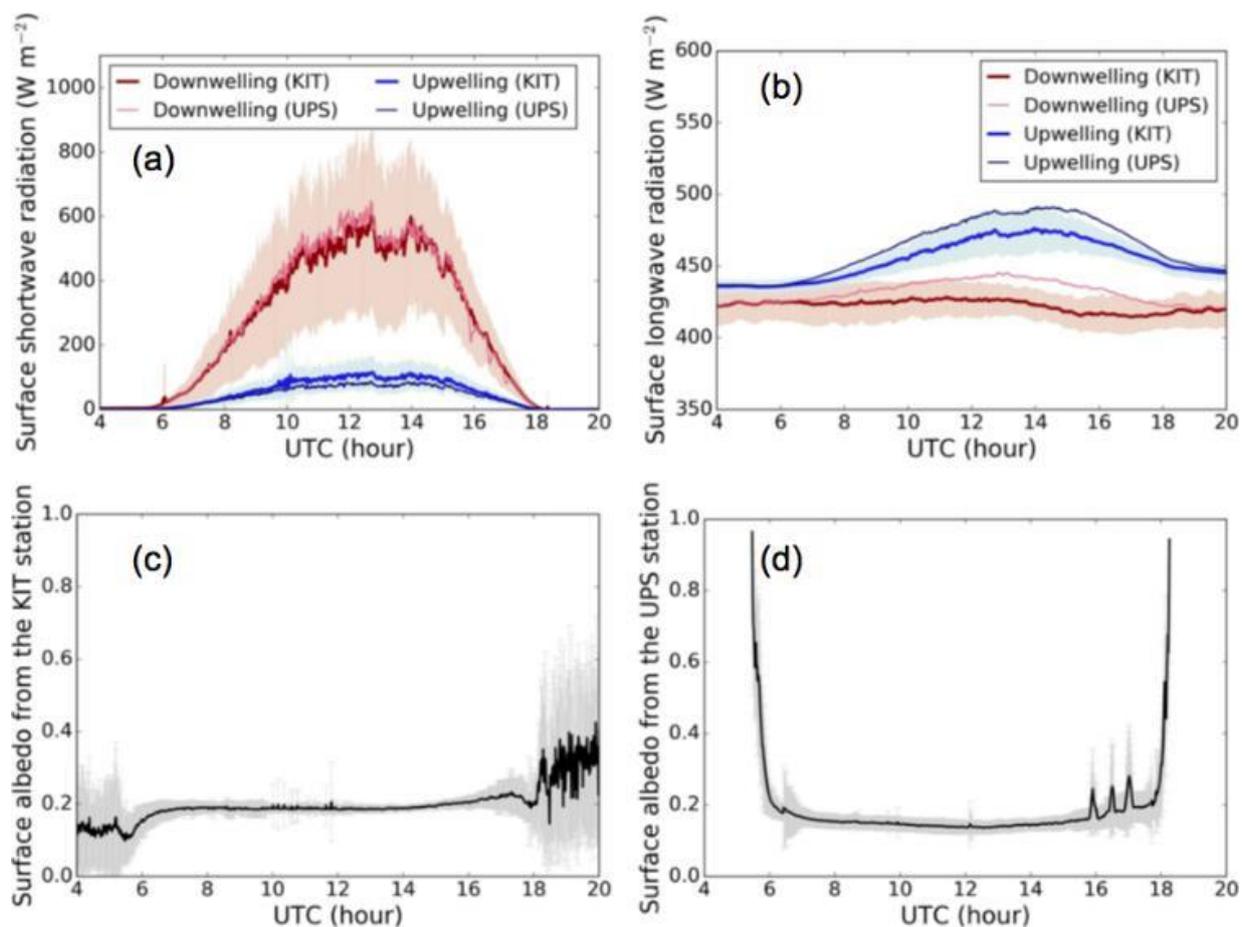

Fig 1. Composite surface shortwave (a) and longwave (b) downwelling and upwelling mean irradiance from the KIT and UPS stations during 1 June –30 July 2016. Shaded areas represent one standard deviation in the means using KIT measurements. The corresponding mean surface albedo from the KIT and UPS stations are shown in (c) and (d), respectively.

2.2 The Ensemble Cloud Retrieval (ENCORE) method

Using synergistic measurements of radar, lidar and shortwave zenith radiance, we retrieve cloud microphysical and optical properties based on the Ensemble Cloud Retrieval (ENCORE) method [*Fielding et al.*, 2014; 2015]. ENCORE has several strengths, including full error statistics of retrieval, the ability to incorporate 3D radiative transfer into the retrieval process, and the flexibility to include any additional observations.

The state vector (i.e., retrievable variables) in ENCORE includes a height-invariant cloud droplet number concentration, and vertically resolved water content and droplet effective radius of clouds. The best estimate of the state vector is found via an iterative ensemble Kalman filter, given as:

$$\boldsymbol{x}_{i+1} = \boldsymbol{x}_i + \mathbf{K}\big(y - h(\boldsymbol{x}_i)\big) - (1 - \mathbf{K}\mathbf{H}_i)(\boldsymbol{x}_i - \boldsymbol{x}_b), \qquad (1)$$

where $\boldsymbol{x}_i$ and $\boldsymbol{x}_{i+1}$ are the current and updated state vectors, respectively; $\boldsymbol{x}_b$ is the background of the state vector; y is the observation; $h(\boldsymbol{x}_i)$ is the forward model with $\mathbf{H}_i$ its linearization. $\mathbf{K}$ is the Kalman gain that controls how much weight is placed on the observations compared to the current state. The initial guess and uncertainty used in the retrieval are summarised in Table 1; details about the underlying assumptions of cloud droplet size distribution, forward model, and calculations of $\mathbf{K}$ can be found in *Fielding et al.* [2014, 2015].

The advantage of the iterative ensemble approach is that the sensitivity of the state to the observations are determined directly from the sample correlations; specifically, both $\mathbf{K}$ and $\mathbf{H}_i$ can be approximated using the spread in ensemble states, the spread in predicted observation values, and the observation and forward model error covariance (as derived in *Gilijns et al.*, 2006). This allows us to bypass direct calculations of the Jacobian of the forward model (i.e., the sensitivity of the forward model to its input), which is difficult in the case of 3D radiative transfer. Note that $\mathbf{H}$ is similar to the Jacobian, but not the same. The Jacobian is the exact derivative of the forward model with respect to the state, while $\mathbf{H}$ can be considered as an approximate derivative calculated from the ensemble states and observations directly. Additionally, the error covariance of the initial ensemble state can be considered as the background error and thus is included in $\mathbf{K}$.

Note that Eq. (1) is slightly different from the method reported in *Fielding et al.* [2014], with the inclusion of the last term on the right hand side, which represents how much $\boldsymbol{x}$ changes because of the mismatch between the current state and the background. In the version of *Fielding et al.* [2014], we performed iterations using the same observations until the forward modelled values fitted the observations to a specified tolerance, effectively losing the information of the background during the iterative process. Since the background is chosen from the climatological mean with a sufficiently large initial uncertainty, it has little influence on the final solution, and thus loses its information during iterations. However, without the last term, the error estimate would become zero after a sufficient number of iterations. To ensure correct and consistent error estimates, we have included the last term (as proposed in *Gu and Oliver*, 2006) to make ENCORE more similar to a standard Gauss-Newton iterative method. In the new version of ENCORE, even though the background remains to play a minor role in determining the best estimate of $\boldsymbol{x}$, it will not be completely neglected and the retrieval error estimate will be appropriate no matter how many times of iterations are performed.

2.3 Ancillary data

ENCORE retrieval is evaluated against four independent observation datasets. Firstly, the total liquid water path (LWP) is compared to that inferred from the microwave radiometer (MWR). MWR measures brightness temperatures in the frequencies of 20–30, 50–60 and 90 GHz with 1-sec temporal resolution, operated in a combination of various scan modes and vertical stare mode. For intercomparison purposes, we use LWP from vertical stare mode only, which is typically 20-min long and available every 30 min. Integrated water vapour and LWP are retrieved using an algorithm provided by the University of Cologne [*Löhnert and Crewell*, 2003; *Löhnert et al.*, 2009]. The algorithm has been trained by more than 12,000 radiosonde profiles measured at Abidjan, Ivory Coast, between 1980 and 2014.

Table 1. *Initial guesses and their associated uncertainties used in ENCORE.*

Observation / Parameter	Value	Uncertainty (1 s.d.)
Radar reflectivity (dBZ)[a]	Cloud radar data	0.5 dBZ
Lidar attenuated backscatter $(1 \ sr^{-1}m^{-1})$	Ceilometer data	12%
Zenith radiance (W m^{-2} μm^{-1} sr^{-1})	Cloud mode data	2.5 %
Surface albedo		
440 nm	0.04	10 %
870 nm	0.31	5 %
1640 nm	0.27	5 %
Cloud		
Logarithmic cloud droplet number concentration (N_c; cm^{-3})	$\log_{10} 100$	0.5
Logarithmic cloud liquid water content (g m^{-3})	$\log_{10} 0.5$	0.5

Secondly, the optical depth is compared to that inferred from the zenith radiance measurements (see *Chiu et al.*, 2010). Note that since the same zenith radiance measurements are used in ENCORE, good agreement in cloud optical depth intercomparison is expected, except the situation that the ENCORE is unable to find solutions that converge to the observed zenith radiance.

Thirdly, we perform a closure study for surface shortwave radiation, using the Suite Of Community RAdiative Transfer codes based on Edwards and Slingo (SOCRATES; *Edwards and Slingo*, 1996). The radiation calculations are performed in one-dimension (1D), assuming plane-parallel, homogeneous clouds from ENCORE retrieval. For each profile, since ENCORE retrieval is available only for warm clouds up to 5 km, the radiative effects of clouds above 5 km are not included in the current radiation calculations. Additionally, the atmospheric profile below 20 km was taken from radiosonde measurements, while ERA-Interim provides pressure, temperature, and humidity above 20 km, as well as ozone for the whole depth of the atmosphere. Linear interpolation is used to map these variables onto the ENCORE vertical grid below 5 km and the ERA-interim vertical grid above. Other gases such as CO_2, CH_4, N_2O, and O_2 have constant mixing ratios in the vertical throughout the calculations. As mentioned in Section 2.1, a mean surface

albedo of 0.19 is derived from surface radiation stations (see Fig. 1) and is used in radiative transfer calculations. In the longwave spectral region, we assume the surface emissivity to be 1.0. Finally, since detailed aerosol profiles are not available yet, the current calculations do not include aerosols, but results will be updated once we have better knowledge on aerosol microphysical and optical properties.

Fourthly, the cloud retrieval is compared with in-situ cloud measurements. Cloud size distributions measured from the Cloud Droplet Probe (CDP) on the Twin Otter, provided by WP4 (University of Manchester), is used to evaluate the ENCORE-retrieved cloud water content and effective radius. Cloud statistics were calculated using in-situ data points where the Twin Otter flew within 1°x 1° domain with a centre of Savé.

3.   Cloud retrieval from ENCORE

ENCORE retrieval is provided with a 10-sec resolution and 30-m vertical resolution. Retrieval includes cloud droplet number concentration (height-independent), cloud water content and effective radius, cloud optical depth and total water path. Their associated retrieval uncertainty is estimated by one standard deviation of 100 ensemble members. Observations used in the retrieval process are also included in the product. For each profile, a quality flag can be found, detailing the corresponding condition (e.g., no cloud detected; all observations are available and the cloud retrieval is successful; lidar measurements were missing; etc.)

3.1   Overcast-to-cumulus transition on 6 July

Clouds on 6 July 2016 represent a typical case during the campaign: low clouds were observed at nighttime and started breaking up in the afternoon, as indicated in ceilometer backscatter signals (Fig. 2). Compared to other days during the campaign, this case has much fewer mid- and high-level clouds during 8:00 – 18:00 UTC. Since we focus on low cloud retrieval, the lack of higher-level clouds helps minimise their impact on radiative transfer calculations for surface radiation, and can ensure that the retrieval performance of low clouds is appropriately evaluated. This case also provides an opportunity to investigate the retrieval performance of ENCORE for small, scattered cumulus clouds in the afternoon.

In general, droplet number concentration of the daytime overcast clouds is around 100 – 200 cm^{-3}; cloud effective radius is ~5 μm and has little variation. LWP ranges between 100 – 150 g m^{-2}, and agrees very well with those retrieved from MWR. In contrast, cloud optical depths vary significantly during daytime, but remain to agree well with those retrieved from cloud mode observations; this indicates that the forward modelled radiance has converged to the observed radiance nicely. Compared to stratiform clouds prior to 13:00 UTC, scattered cumulus during 14:00 – 18:00 UTC have similar cloud effective radius, but the number concentrations are much lower, resulting small optical depths of ~ 5–10.

The drop number concentration retrieved in this case appears low, considering the DACCIWA region where has rich mix of natural and anthropogenic aerosols. After checking lidar depolarisation ratio (indicating particle shape), the layer above clouds at 8–12 UTC (with around –40 dBZ reflectivity) is likely due to insects. It is not typical to have insects above clouds, but it seems to be common at this site. Therefore, we are currently looking into the best way to identify insects properly. Once insect returns are removed, the cloud geometric thickness will decrease; as a result, the droplet number concentration will likely increase in order to achieve the same optical depth and LWP.

The observed and computed SW downwelling irradiances at surface are shown in Fig. 3. In general, ENCORE retrieval generates surface radiation following similar variations to observations, particularly in the early morning between 6–9 UTC. For complex cloud fields in 9–13 UTC, many cloud retrievals capture the radiation variations, but a significant amount of calculated irradiances are lower than observations. It is unclear yet if the discrepancy is due to overestimated cloud water content, or due to the cloud inhomogeneity issue in radiative transfer calculations. We will look into the variations of clouds and radiation measurements at a 10-sec temporal resolution (rather than 1-min) to pin down the sources of the radiation errors.

Fig 2. Retrieved cloud properties on 6 July 2016 during the DACCIWA campaign. Panels from top to bottom show time series of observed cloud radar reflectivity factor (for 0–15 km and a zoom-in for 0–5 km), ceilometer backscatter, and zenith radiances; and retrieved cloud water content, cloud effective radius, cloud droplet number concentration, total water path, column-mean effective radius, and column-integrated cloud optical depth. Liquid water paths retrieved from microwave radiometer measurements (magenta dots), and cloud optical depths from cloud mode (red (more reliable) and green dots (with relatively higher uncertainty)) are also co-plotted. The blue shading represents one standard deviation uncertainty in the retrieval (although it may be too small to show).
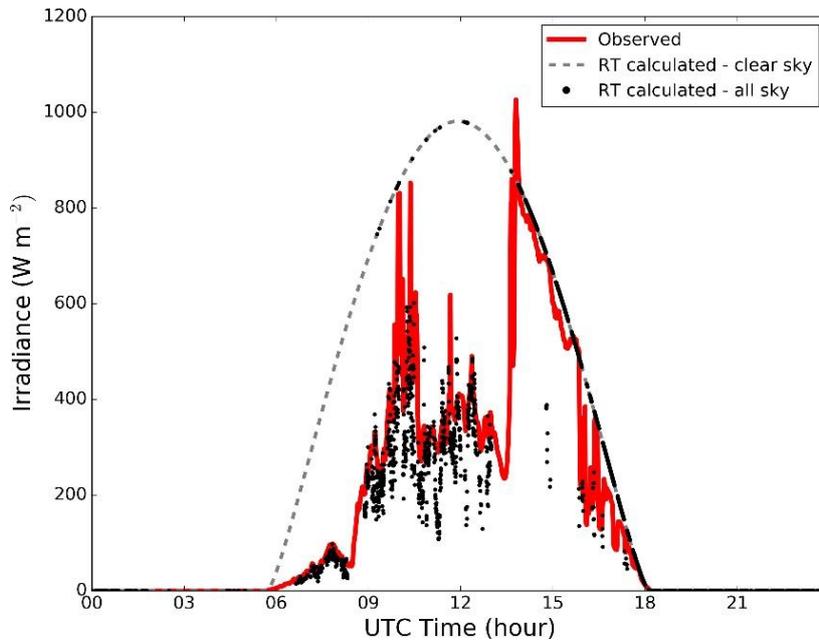
Fig 3. *Time series of surface SW downwelling irradiance on 6 July 2016, from observations (red) and radiative transfer calculations using ENCORE cloud retrieval as input (black dots). The corresponding clear-sky irradiance is co-plotted by grey dashed lines.*

3.2 Overcast low clouds

Overcast low clouds were observed on 5 July 2016, from both sky images and ceilometer backscatter signals (as shown in Fig. 4). Cloud gaps appear shortly before 8:00 UTC, but become optically thick again after 8:00 UTC. Based on radar reflectivity and sky images, cirrus clouds were present at 10–14 km altitude throughout the entire day, except 11:30 – 14:00 UTC. Between 8:00 – 14:00 UTC, mid-level altocumulus clouds were observed at ~5 km altitude. Additionally, cloud radar reflectivity indicated a short shower later on at 17:00 UTC, but precipitation was not heavy enough to reach the ground.

Similar to the previous case, the retrieved cloud droplet number concentrations are in the order of 100 cm^{-3} and likely increase once we remove insect returns; cloud effective radius is about 6–8 µm and again remains surprisingly constant throughout the day. The mean cloud optical depth is 22 and the mean LWP is 96 g m^{-2}. Compared to MWR-retrieved LWP, ENCORE retrieval tends to be larger by 20 g m^{-2}. Although this difference is within the retrieval uncertainty of 20–30 g m^{-2} in MWR retrieval [*Marchand et al.*, 2003; *Crewell and Löhnert*, 2003], a further detailed analysis will be performed to see if such a difference persists in June–July 2016.

Similar to the previous case, the overall variations of calculated irradiances on 5 July are close to observations (as shown in Fig. 5). While the overall agreement is improved compared to the case on 6 July, there are several irradiance "dips" throughout the day, which were not found in the observed irradiances. Note that the observed irradiance in Fig. 5 is 1-min average from the native 1-sec measurements. It would be necessary to look into those 1-sec measurements to understand the role of the inhomogeneity and the evolution in clouds in contributing the discrepancy between the calculated and observed irradiances.
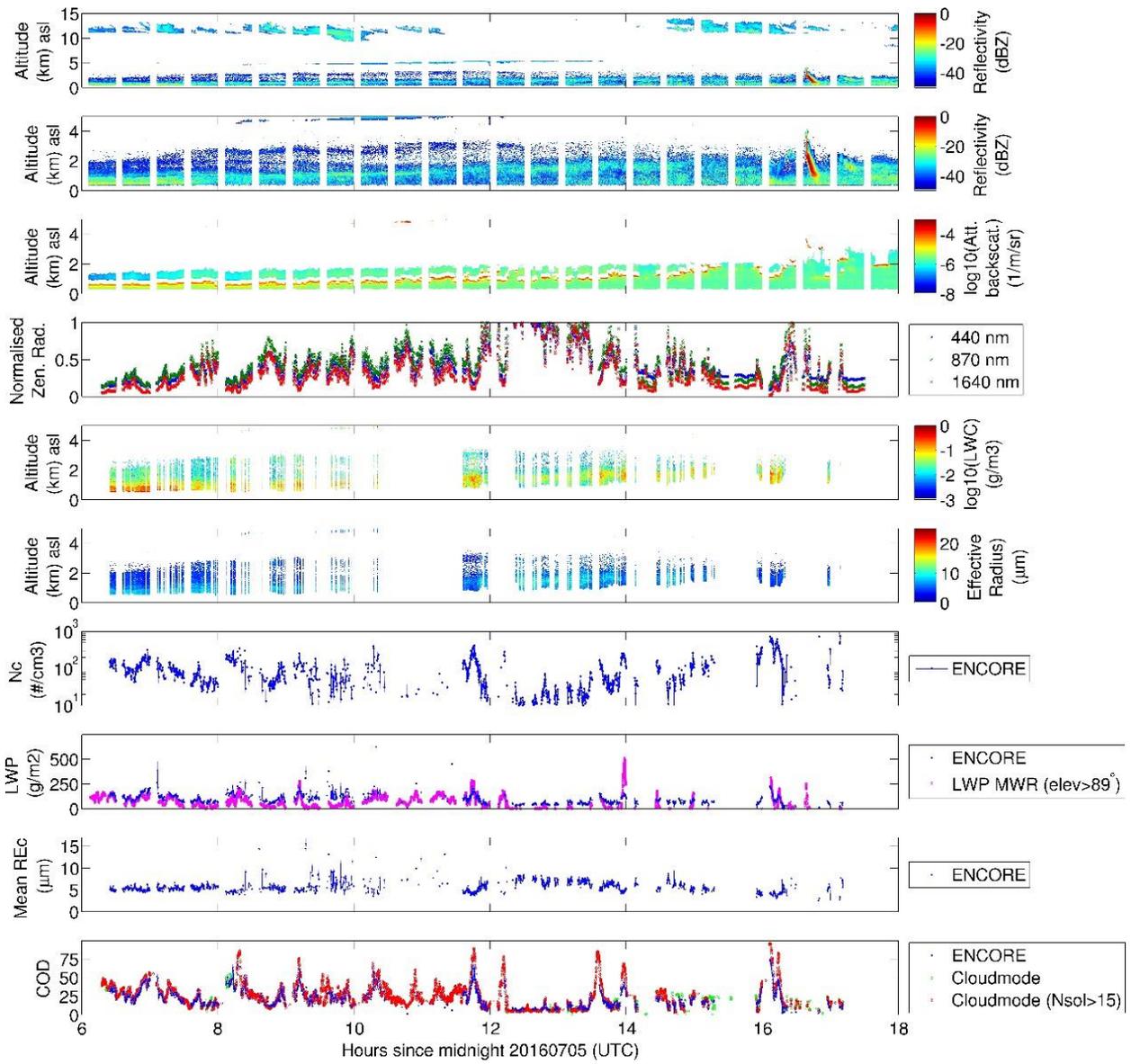
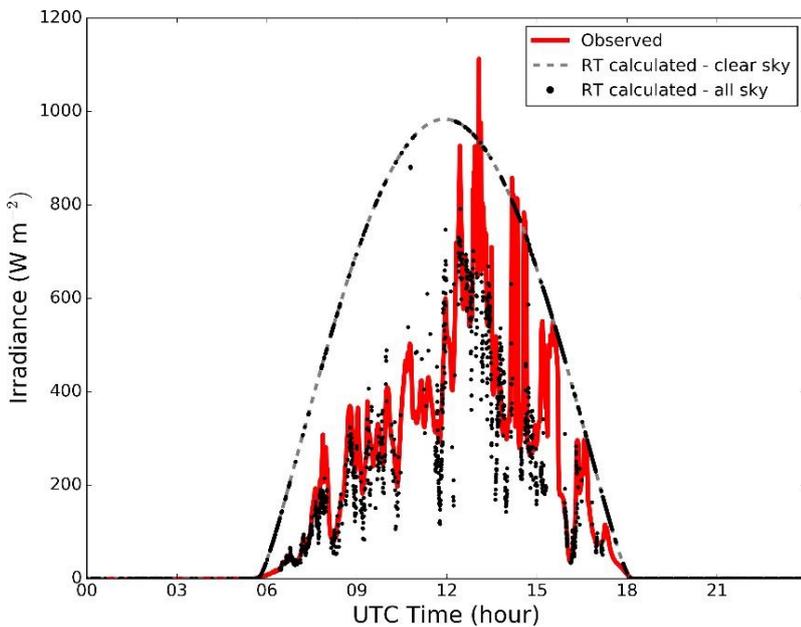**Fig 4.** *Same as Fig. 2, but for 5 July 2016.*

Fig 5. *Same as Fig. 3, but for 5 July 2016.*

3.3 7 July

The Twin Otter flew over Savé on 3 and 7 July; in particular, the flight on 7 July provides more samples for us to evaluate ENCORE retrieval (Fig. 6). During 10:30–11:00, the aircraft flew at altitudes of ~0.4–1.5 km, with mean cloud effective radii ranging from 5±4 µm at 0.5 km to 3±2 µm at 1.5 km.
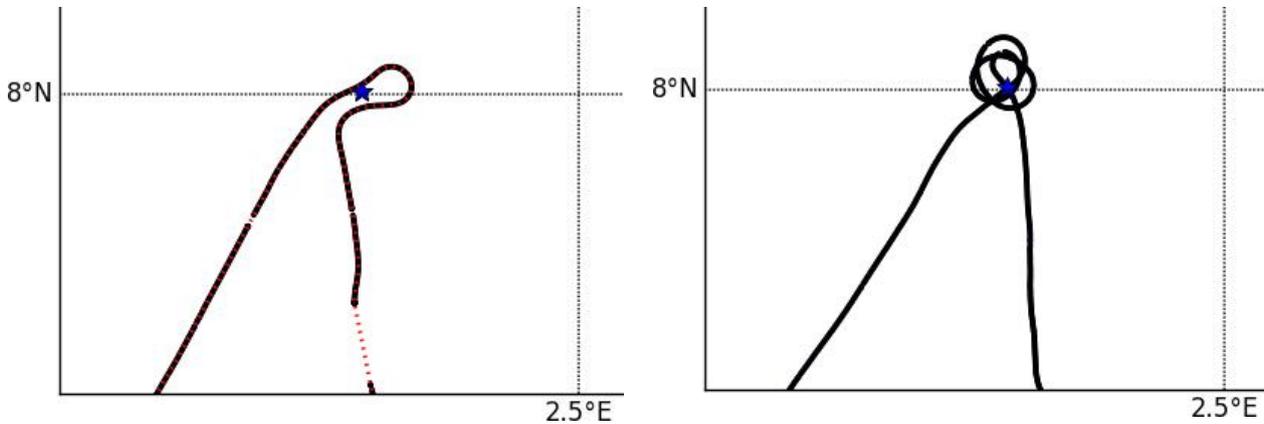

Fig 6. Flight tracks of the Twin Otter on 3 (left) and 7 (right) July 2016. The location of Savé is represented by the blue star.

ENCORE retrieval and the corresponding calculated surface irradiance are shown in Figures 7 and 8. Similar to previous cases, ENCORE retrieval generally agrees well with that from MWR and that from cloud mode observations. The ENCORE-retrieved cloud effective radius is also about 5 µm, which is consistent with in-situ measurements. Interestingly, although we have good agreement between retrieval and in-situ measurements during 10:30–11:00, we find that's when one of the irradiance "dips" occurred. It is planned to look into the detailed cloud size distribution to understand which cloud variable in ENCORE may have contributed to the radiation discrepancy.

4. Summary and discussions

The preliminary cloud retrieval from the synergistic remote sensing measurements at Savé shows good agreement with aircraft cloud measurements, and leads to surface SW downwelling irradiance that is consistent with measurements from the radiation station. This product will allow us to further investigate detailed cloud statistics; radiative effects of low clouds over the DACCIWA region; the interactions between cloud microphysical and optical properties, dynamics and aerosols; and the potential model biases in clouds.

In the cases presented in this report, it is somewhat surprising that we have not seen high cloud droplet number concentration, as expected in a relatively polluted environment. Doppler lidar data suggested that insects above clouds may have affected our retrieval in droplet number concentration. We are currently working on insect classifications and retrieval will be updated accordingly.

Some periods with high radar reflectivity suggested possible precipitation, but the relatively small cloud effective radius may have prevented these drops from reaching the surface, consistent with the lack of surface precipitation in rain gauge data. We currently treat all clouds as non-drizzling, but will switch the retrieval method to drizzling mode to start retrieving drizzle properties in clouds. This will allow us assess in-cloud warm rain formation and sub-cloud evaporation processes in more detail.
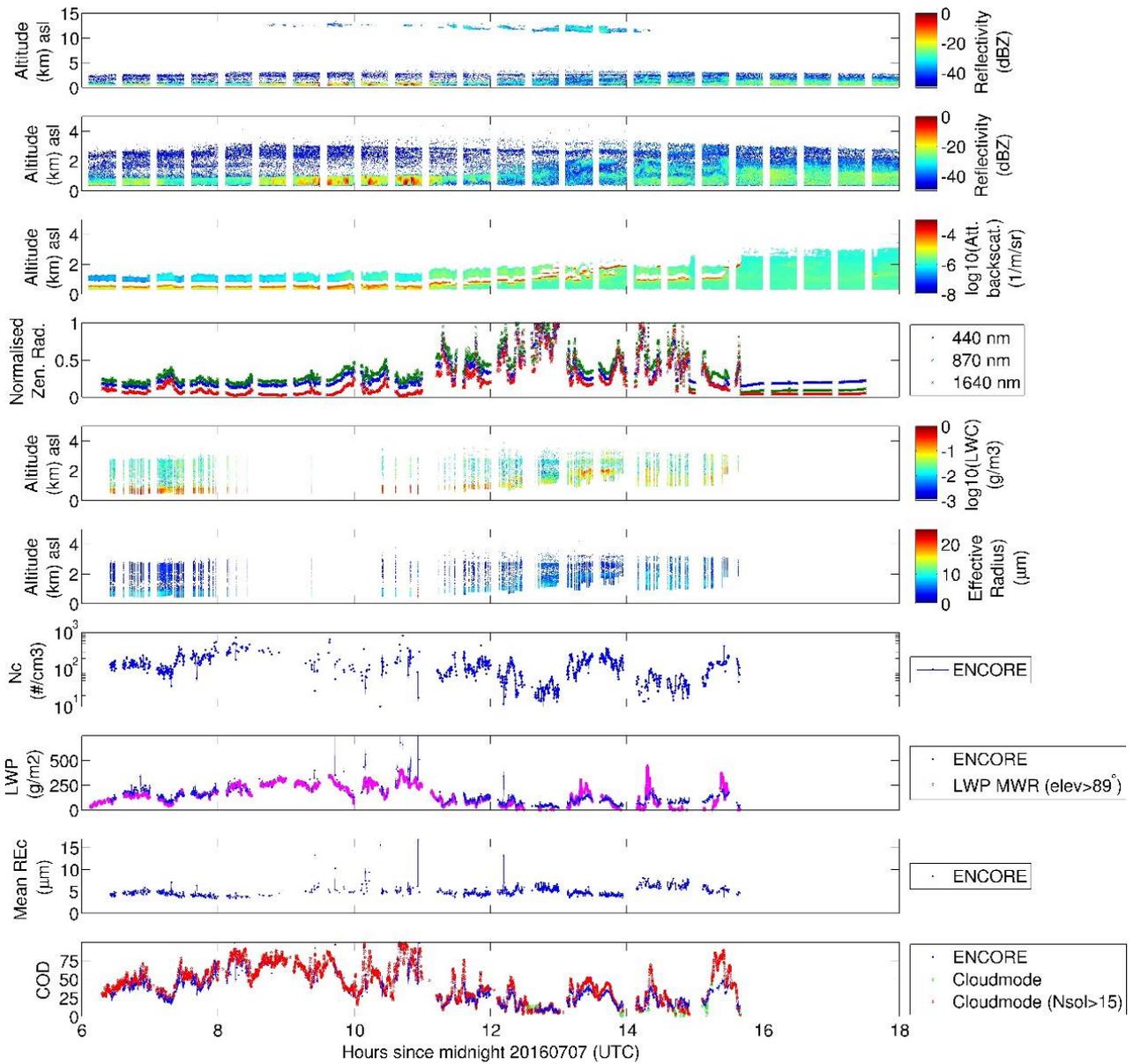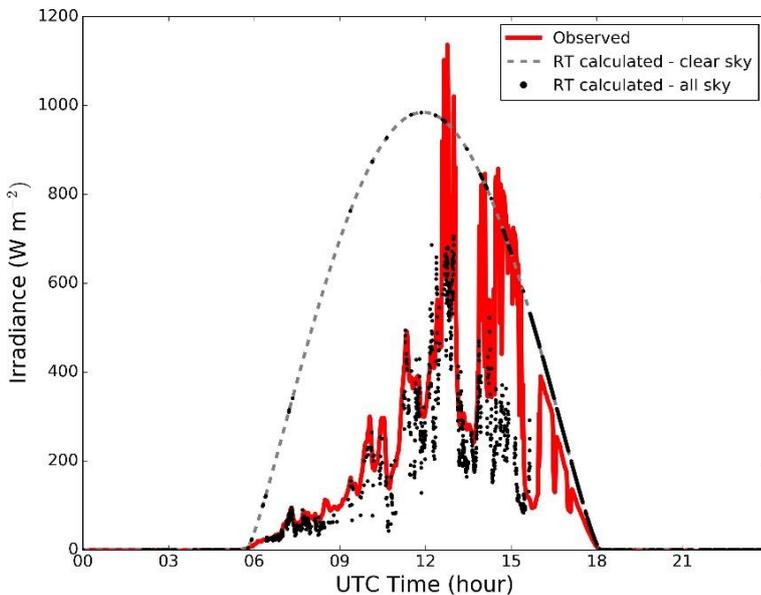
Fig 7. *Same as Fig. 2, but for 7 July 2016.*

Fig 8. *Same as Fig. 3, but for 7 July 2016.*

References

Chiu, J. C., A. Marshak, C.-H. Huang, T. Varnai, R. Hogan, D. M. Giles, B. N. Holben, E. O'Connor, Y. Knyazikhin, W. J. Wiscombe, 2012: Cloud droplet size and liquid water path retrievals from zenith radiance measurements: examples from the Atmospheric Radiation Measurement Program and the Aerosol Robotic Network. *Atmos. Chem. Phys.*, 12, 10313–10329.

Chiu, J. C., C. Huang, A. Marshak, I. Slutsker, D. M. Giles, B. N. Holben, Y. Knyazikhin, and W. J. Wiscombe, 2010: Cloud optical depth retrievals from the Aerosol Robotic Network (AERONET) cloud mode observations. *J. Geophys. Res.*, 115, D14202, doi:10.1029/2009JD013121.

Clothiaux, E., G., Mace, T. Ackerman, T. Kane, J. Spinhirne, and V. Scott, 1998: An automated algorithm for detection of hydrome- teor returns in micropulse lidar data. *J. Atmos. Ocean. Tech.*, 15, 1035–1042.

Edwards, J. M., and A. Slingo, 1996: Studies with a flexible new radiation code. I: Choosing a configuration for a large-scale model. *Quart. J. Roy. Meteor. Soc.*, 122, 689–720.

Fielding, M. D., J. C. Chiu, R. J. Hogan, G. Feingold, E. Eloranta, E. J. O'Connor and M. P. Cadeddu, 2015: Joint retrievals of cloud and drizzle in marine boundary layer clouds using ground-based radar, lidar and zenith radiances, Atmos. Meas. Tech., 8, 2663–2683, doi:10.5194/amt-8-2663-2015.

Fielding, M. D., J. C. Chiu, R. J. Hogan and G. Feingold, 2014: A novel ensemble method for retrieving properties of warm cloud in 3-D using ground-based scanning radar and zenith radiances, *J. Geophys. Res. Atmos.*, 119, doi:10.1002/2014JD021742.

Fielding, M. D., J. C. Chiu, R. J. Hogan and G. Feingold, 2013: 3D cloud reconstructions: Evaluation of scanning radar scan strategy with a view to surface shortwave radiation closure, *J. Geophys. Res.*, 118, 9153–9167, doi:10.1002/jgrd.50614.

Gillijns, S., O. B. Mendoza, J. Chandrasekar, B. L. R. De Moor, D. S. Bernstein, and A. Ridley (2006): What is the ensemble Kalman filter and how well does it work? *Proc. Am. Control Conf.*, 1–12, 4448–4453, doi:10.1109/Acc.2006.1657419.

Gu, Y., and D. S. Oliver, 2006: The ensemble Kalman filter for continuous updating of reservoir simulation models. *J. Energy Resour. Technol.*, 128, 79–87.

Hannak, L., P. Knippertz, A. H. Fink, A. Kniffka, and G. Pante, 2017: Why Do Global Climate Models Struggle to Represent Low-Level Clouds in the West African Summer Monsoon? *Journal of Climate*, 30, 1665–1687.

Knippertz, P., A. H. Fink, R. Schuster, J. Trentmann, J.M. Schrage, and C. Yorke, 2011: Ultra-low clouds over the southern West African monsoon region. *Geophys. Res. Lett.*, 38 (21),

Li, R., J. Jin, S.-Y. Wang, and R. R. Gillies, 2015: Significant impacts of radiation physics in the Weather Research and Forecasting model on the precipitation and dynamics of the West African Monsoon. *Clim Dyn*, 44 , 1583–1594.

Löhnert, U., and S. Crewell, 2003. Accuracy of cloud liquid water path from ground-based microwave radiometry: Part I. Dependency on cloud model statistics and precipitation. *Radio Sci*. 38 (3), 8041.

Löhnert, U., D. D. Turner, and S. Crewell, 2009: Ground-based temperature and humidity profiles using spectral infrared and microwave observations – Part I: simulated retrieval performance in clear-sky conditions. *J. Appl. Meteor. Climatol.*, 48, 1017–1032, 2009.

O'Connor, E. J., R. J. Hogan, and A. J. Illingworth, 2005: Retrieving stratocumulus drizzle parameters using Doppler radar and lidar. *J. Appl. Meteorol.*, 44, 14–27, doi:10.1175/Jam-2181.1.

Rodwell, M. J., and T. Jung, 2008: Understanding the local and global impacts of model physics changes: an aerosol example. *Quarterly Journal of the Royal Meteorological Society*, 134, 1479–1497.